Eur. Phys. J. C 18, 167–179 (2000)
Digital Object Identifier (DOI) 10.1007/s100520000494

THE EUROPEAN PHYSICAL JOURNAL C

Soft diffraction and the elastic slope at Tevatron and LHC energies: a multi-Pomeron approach

V.A. Khoze[1], A.D. Martin[1], M.G. Ryskin[1,2]

[1] Department of Physics, University of Durham, Durham, DH1 3LE, UK
[2] Petersburg Nuclear Physics Institute, Gatchina, St. Petersburg, 188350, Russia

Received: 1 August 2000 / Published online: 27 October 2000 – © Springer-Verlag 2000

Abstract. We present a formalism for high energy soft processes, mediated by Pomerons, which embodies pion-loop insertions in the Pomeron trajectory, rescattering effects via a two-channel eikonal and high-mass diffractive dissociation. It describes all the main features of the data throughout the ISR to Tevatron energy interval. We give predictions for soft diffractive phenomena at the LHC energy, and we calculate the different survival probabilities of rapidity gaps which occur in various diffractive processes.

1 Introduction

At high pp (or $p\bar{p}$) collider energies about 40% of the total cross section $\sigma_{\rm tot}$ comes from diffractive processes, like elastic scattering or single- or double-diffractive dissociation. Besides their interest in their own right, there are several other practical reasons why it is important to study diffractive processes. First, we need to understand the structure of $\sigma_{\rm tot}$ and the nature of the underlying events which accompany the sought-after rare hard processes. Second, we must be able to estimate the probability that rapidity gaps, which occur in diffractive events containing a hard subprocess, survive rescattering effects — that is, survive the population of the gaps by secondary particles from the underlying event. Recall that 'hard' diffraction processes are a means of suppressing the background, for example, in searches for signals of New Physics. Thirdly, studies of diffractive processes should help in understanding the structure of high energy cosmic ray phenomena. Finally, we wish to be able to reliably extrapolate the pp elastic differential cross section $d\sigma_{\rm el}/dt$ to the optical point $t = 0$ so as to make a luminosity measurement at the LHC. Indeed the early low luminosity runs of the LHC should provide a wealth of information on diffractive interactions at small momentum transfer, which will enable asymptotic ($s \to \infty$) predictions to be severely tested. Such small-t processes are generically called *soft* interactions.

The luminosity measurement is based on the optical theorem (neglecting Coulomb effects)

$$\left.\frac{d\sigma_{\rm el}}{dt}\right|_{t=0} = \frac{\sigma_{\rm tot}^2}{16\pi}\,(1+\rho^2). \tag{1}$$

The ratio ρ of the real to the imaginary part of the elastic amplitude is small at Tevatron and LHC energies ($\rho \sim 0.1$), and a dispersion relation estimate is sufficiently accurate for ρ not to cause a problem. Thus if we measure the number of events corresponding to the elastic and to the total cross sections then we may determine both the luminosity $\mathcal{L}$ and $\sigma_{\rm tot}$ (since $N_{\rm el} \propto \sigma_{\rm tot}^2\mathcal{L}$, whereas $N_{\rm tot} \propto \sigma_{\rm tot}\mathcal{L}$). The main difficulty is that, at the LHC, we will have to extrapolate elastic data from, say, $|t| \gtrsim 0.01$ GeV^2 to $t = 0$. It is found, from measurements at ISR, S$p\bar{p}$S and Tevatron energies, that the 'local' slope

$$B(t) \;=\; \frac{d(\ln d\sigma_{\rm el}/dt)}{dt} \tag{2}$$

depends on t. The effect is not negligible. For example, at $\sqrt{s} = 53$ GeV [1]

$$B(0) \;-\; B(|t| = 0.2\ {\rm GeV}^2) \;\simeq\; 2\ {\rm GeV}^{-2}. \tag{3}$$

Here we will study such effects.

It is important to pay special attention to the periphery of the proton, in impact parameter, b_t, space. First, large values of b_t are responsible for the small t behaviour of the amplitude. Second, the large b_t region, where the optical density (or opacity), $\Omega(b_t)$, becomes small, gives the major contribution to the survival probability of rapidity gaps.

The outline of the paper is as follows. In Sect. 2 we very briefly recall the role of the Pomeron in describing high energy soft interactions. Then in Sect. 3 we list the essential ingredients to be embodied in a model for the Pomeron. We present an old, but important, result [2] which gives the effect of pion-loop insertions on the Pomeron trajectory. Section 4 discusses the form of the Pomeron-proton vertex and incorporates screening corrections in the model. All the above effects leads to a t dependence of the elastic slope parameter B of (2). For pedagogic reasons, it is informative to first attempt a preliminary description of the pp total cross section and $d\sigma_{\rm el}/dt$ data using a model which embodies the above effects but

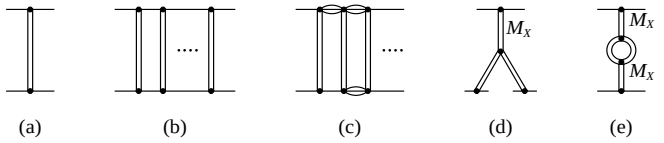

Fig. 1a–e. The Pomeron exchange contribution, graph **a**, together with unitarity corrections, graphs **b–e**, to the pp elastic amplitude. Note that graphs (d, e) are the 'square' of the single- and double-diffractive dissociation amplitudes respectively

which, for the moment, neglects the effects of high-mass diffraction dissociation. The comparison of this incomplete Pomeron model with the data is also described in Sect. 4. Then in Sect. 5 we discuss the inclusion of diffractive dissociation in the analysis. Section 6 presents the resulting, much more complete, theoretical description of the data. Predictions of soft phenomena at LHC energies are made. Section 7 describes the calculation of the probabilities that the rapidity gaps, which occur in various diffractive processes, survive the effects of rescattering. Section 8 contains our conclusions and summarises some of the predictions for soft processes at the LHC.

2 The Pomeron

To introduce our approach, it is helpful to first briefly recall salient points in the long history of the description of elastic and diffractive scattering at small momentum transfer. The high energy behaviour of scattering amplitudes in the small t domain is described by Regge theory (see, for example, [3]), that is by the singularities of the amplitudes in the complex angular momentum, j, plane. The simplest possibility is to assume that, *at high energy*, the diffractive processes are driven by an isolated pole at $j = \alpha(t)$, which gives an elastic amplitude

$$A(s,t) \ \propto \ s^{\alpha(t)}, \tag{4}$$

and a total cross section

$$\sigma_{\rm tot} \ \propto \ s^{\alpha(0)-1}. \tag{5}$$

The pole with the largest intercept, originally with $\alpha(0) = 1$, was called the Pomeron. Here we are interested in energies $\sqrt{s}$ which are sufficiently large to be able to neglect all secondary trajectories (with intercepts of $\alpha(0) \lesssim 0.5$). The Pomeron is shown in Fig. 1a by the double line, which is exchanged in the t-channel in pp elastic scattering.

However this description is too simplified. The imposition of s-channel unitarity generates multi-Pomeron cuts from the pole in the j-plane. First, iterations of the pole amplitude via elastic unitarity gives contributions of the type shown in Fig. 1b. If we take account of the possibility of proton excitations ($p \to N^*$) in intermediate states, then we must include contributions such as that in Fig. 1c. Furthermore, the excitation into higher mass M_X states is described by the triple-Pomeron graph of Fig. 1d for single diffractive dissociation (with cross section $\sigma_{\rm SD}$) and by Fig. 1e for double diffractive dissociation ($\sigma_{\rm DD}$). In addition to Fig. 1d, there is an equal contribution $\sigma_{\rm SD}$ from dissociation of the lower proton only. The contributions of graphs 1(b–e) are not negligible. Indeed, from the AGK cutting rules [4] we estimate the correction to Fig. 1a to be

$$(\sigma_{\rm el} + 2\sigma_{\rm SD} + \sigma_{\rm DD})/\sigma_{\rm tot} \ \sim \ 0.4 \tag{6}$$

at Tevatron/LHC energies, which is consistent with the Tevatron data.

Of course, it is possible to consider an effective or phenomenological 'Pomeron'-pole amplitude which includes, in an average sense, all the cuts shown in Figs. 1b–e. Indeed, it has been demonstrated, by Donnachie and Landshoff [5], that a simple pole with trajectory

$$\alpha_{\rm eff}(t) \ = \ 1.08 \ + \ 0.25\, t \tag{7}$$

(with t in GeV^2) provides a good description of the total and elastic differential cross section data up to the Tevatron energy. However in this case we cannot use the 'Pomeron' to calculate the survival probability S^2 of the rapidity gaps or the small t behaviour of the elastic slope $B(t)$ of (2). The survival probability $S^2 = 1 - W^2$ is small since secondary particles produced in the inelastic interaction fill the gap, with probability W^2. The difficulty is that the effective 'Pomeron' describes a pp amplitude, with an elastic and inelastic component, where the latter component includes diffractive dissociation. Elastic rescattering does not populate the gap and, unfortunately, the effective 'pole' picture does not quantify the size of the dissociation component. Another problem of the effective pole description concerns the t (or b_t) dependence of the elastic amplitude. Each component of the elastic amplitude shown in Fig. 1 has its own characteristic t dependence. For example, if the amplitude for Fig. 1a has the form $\exp(B_0 t/2)$, then the amplitude for the two-Pomeron part of Fig. 1b has a flatter t dependence of the form $\exp(B_0 t/4)$. It was discussed in [6] that the part of $d\sigma_{\rm el}/dt$, which is generated via the optical theorem from diffractive dissociation, should have a larger t-slope since it corresponds mainly to the large b_t or peripheral part of the interaction. These effects are important in the computation of the t dependence of the slope B of (2), as well as for the estimation of survival probability S^2.

3 Model for the Pomeron

Unfortunately, to our knowledge, no way has been found to sum up all the Regge graphs and to solve Regge Field Theory. Here we construct a model of the Pomeron which, at the very least, accounts for the most important effects. We incorporate

(i) s-channel unitarity with elastic and a low mass M_X intermediate state via a 2-channel eikonal approach (using a representative effective low mass proton excitation N^*),

(ii) high-mass M_X single- and double-dissociation via Figs. 1d and 1(e)[1],

[1] The data indicate that the "effective" triple-Pomeron vertex (which already includes some absorptive corrections) is

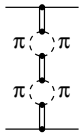

Fig. 2. A two pion-loop insertion in the Pomeron trajectory, generated from the single loop by t-channel unitarity

(iii) the nearest t-channel singularity, that is the two-pion loop.

In high energy 'soft' strong interactions we deal with two different hadronic scales. One is given by the mass of the pion and controls the periphery of the proton — the so-called pion cloud — see (iii) above. Due to the pseudo-Goldstone nature of the pion, this scale (m_π) is rather small. For the same reason, pion exchange is not the most important part of the interaction amplitude. At small distances the interaction is controlled by a scale $m \sim 1$ GeV representative of the other hadron masses[2].

Long ago, Anselm and Gribov [2] argued that the Pomeron is built up from both the small and large scale components. The large scale (small b_t) component gives the main contribution to the Pomeron, which may be described by a simple *bare* pole with trajectory

$$\alpha(t) \;=\; \alpha(0) \;+\; \alpha' t. \tag{8}$$

The other component, the pion-loop insertions of the type shown in Fig. 2, generated by t-channel unitarity, may be treated as a correction. They are needed to describe the large b_t region. Following Anselm and Gribov [2], we find that these pion-loop corrections modify the Pomeron trajectory so as to give the non-linear form[3]

$$\alpha_{I\!P}(t) \;=\; \alpha(0) \;+\; \alpha' t \;+\; \frac{\beta_\pi^2 m_\pi^2}{32\pi^3}\, h\left(\frac{4m_\pi^2}{|t|}\right), \tag{9}$$

where

$$h(\tau) = -\frac{4}{\tau}\, F_\pi^2(t)\, \left[2\tau \;-\; (1+\tau)^{3/2}\, \ln\left(\frac{\sqrt{1+\tau}+1}{\sqrt{1+\tau}-1}\right) + \ln\frac{m^2}{m_\pi^2}\right], \tag{10}$$

with $\tau = 4m_\pi^2/|t|$ and $m = 1$ GeV. The coefficient β_π^2 specifies the $\pi\pi$ total cross section, and $F_\pi(t)$ is the form factor of the pion-Pomeron vertex. The coefficient $\beta_\pi^2 m_\pi^2/32\pi^3$ in (9) is small, but due to the tiny scale m_π the t dependence of $h(\tau)$ is steep and non-linear. It has an important effect on the local slope $B(t)$ of (2). In fact it was shown [2] that, with a reasonable $\pi\pi$ total cross section, it can account for at least half of the slope difference, (3), observed at ISR energies.

For the results that we obtain below for the Pomeron trajectory, $\alpha_{I\!P}(t)$, it is important to note that expression (10) for $h(\tau)$ has been renormalized [2], such that

$$h(\tau) \;=\; h_\pi(\tau) \;-\; h_\pi(t=0) \tag{11}$$

where $h_\pi(\tau)$ denotes the full pion-loop contribution. The value of $h_\pi(0)$ is determined by the region of t that is controlled by the scale m. It therefoire causes an increase of about 0.1 in $\alpha(0)$, depending on the exact slope of the pion form factor, as we go from (8) to (9).

4 Results for the Pomeron — a first look

For simplicity we first compute the Pomeron assuming that the effects of single- and double-diffractive dissociation are negligible. These diffractive effects are incorporated in the results presented in Sects. 5 and 6.

We start from the two-component bare Pomeron (associated with hadronic scales m and m_π) that was discussed above. Once the proton-Pomeron vertex V is specified, the elastic pp amplitude is generated by the optical theorem from the inelastic processes (Fig. 1a). From this bare Pomeron we produce, via s-channel eikonalisation, both elastic and inelastic pp interactions (see Fig. 1b). In practice we use a two-channel eikonal which allows us to simultaneously incorporate $p \to N^*$ diffractive dissociation. In this way we construct a Pomeron whose parameters may be tuned to describe $\sigma_{\rm tot}$ and $d\sigma_{\rm el}/dt$ data throughout the ISR to Tevatron energy range.

The parameters of the Pomeron are $\alpha(0), \alpha'$ of the trajectory (9), and a_1 and a_2 of the elastic proton-Pomeron vertex, which is taken to have the power-like form

$$V(p \to p) \;\equiv\; \beta(t) \;=\; \frac{\beta_p}{(1-t/a_1)(1-t/a_2)}, \tag{12}$$

where β_p^2 specifies $\sigma_{\rm tot}$. The power-like, rather than an exponential, form is motivated by the quark counting rules and by $d\sigma_{\rm el}/dt$ data. The latter is particularly true at ISR energies where multi-Pomeron effects are still reasonably small — as mentioned above, the pion-loop insertions account for about one half of the variation of the local elastic slope $B(t)$ with t, at small t. The power-like form of (12) is needed to account for the remaining change of $B(t)$.

In addition to the above parameters, we also have to specify

$$\gamma \;\equiv\; \frac{V(p \to N^*)}{V(p \to p)}, \tag{13}$$

which we take to be $\gamma \sim 0.4$ in accordance with $p \to N^*$ dissociation observed at moderate energies [10]. We use the additive quark model relation, $\beta_\pi/\beta_p = 2/3$, to determine β_π, and we take the form factor of the pion-Pomeron vertex to have the form

$$F_\pi(t) \;=\; 1/(1-t/a_2). \tag{14}$$

small, namely that the high energy Pomeron-proton and proton-proton total cross sections satisfy $\sigma_{I\!Pp}/\sigma_{pp} \sim 1/40$ [7, 8]. Thus we anticipate that graphs that are higher order in the triple-Pomeron vertex may be neglected.

[2] In terms of QCD the scale $m \sim 1$ GeV may be associated with the 'effective' gluon mass or with the instanton size. Other arguments in favour of a small gluon-gluon correlation length ~ 0.3 fm (or scale ~ 1 GeV) can be found in [9].

[3] Note that in (10) we have corrected the misprint which occurs in the published version of [2].

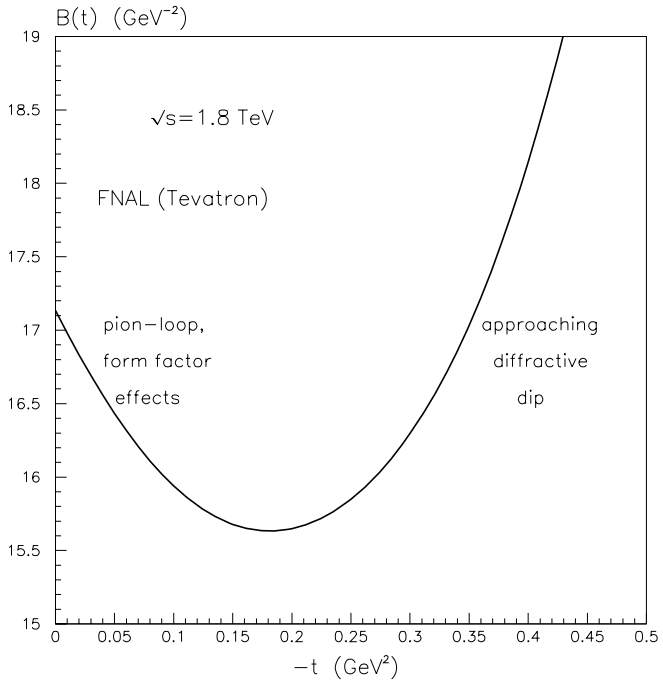

Fig. 3. Typical t dependence of the elastic slope $B(t)$ of (2) found in the model of the Pomeron introduced in Sect. 3. The diffractive dip, arising from the destructive interference between the Pomeron pole and cut contributions, is located at smaller $-t$ for higher collider energies $\sqrt{s}$. The effect on $B(t)$ is seen from the dashed curves in Fig. 9. The inclusion of high-mass diffraction in Sects. 5 and 6 modifies the behaviour of $B(t)$ in the dip region, again see Fig. 9

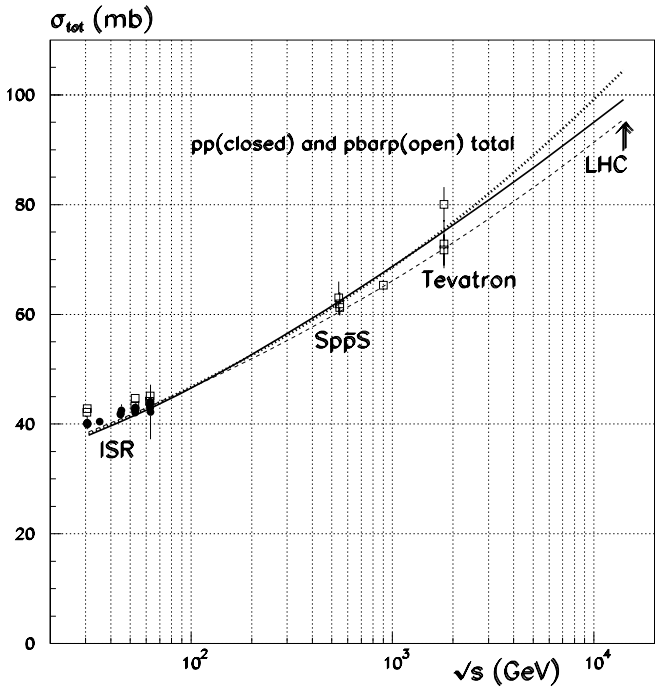

Fig. 4. The model descriptions of high energy pp (or $p\bar{p}$) total cross section data [12]. The continuous, dotted and dashed curves correspond, respectively, to the minimal, maximal diffractive models and to the model of the Pomeron in which high-mass diffraction is neglected. The discrepancy between the curves and the data at the lower ISR energies is entirely due to our neglect of the (secondary) meson Regge trajectories

In summary, we have expressed the t dependence of the elastic pp (or $p\bar{p}$) differential cross section, $d\sigma_{\rm el}/dt$, in the form $\exp(Bt)$, and have argued that the slope B depends on t, even for small t. Actually there are three sources of the t dependence of the elastic slope B:

(i) the pion-loop insertions in the Pomeron trajectory, (9),
(ii) the non-exponential form of the proton-Pomeron vertex $\beta(t)$ of (12),
(iii) the absorptive corrections, associated with eikonalization, which lead to a dip in $d\sigma_{\rm el}/dt$ at $|t| \sim 1$ GeV^2, whose position moves to smaller $|t|$ as the collider energy, $\sqrt{s}$, increases.

The typical t structure of the slope $B(t)$ is shown in Fig. 3. The first two effects are responsible for the initial decrease of the elastic slope as $-t$ increases away from $t = 0$, while the third effect produces a rapid growth of B as $-t$ approaches the position of the diffractive minimum.

To account for s-channel unitarity, (iii), we use a two channel (p, N^*) eikonal formalism [11], as described in Appendix A. For the opacity $\Omega(s, b_t)$ we take the Fourier transform of the Pomeron exchange amplitude

$$A_{I\!P}(t) \;=\; \beta(t)^2 \left(\frac{s}{s_0}\right)^{\alpha_{I\!P}(t)}, \qquad (15)$$

where $\beta(t)$ is given by (12) and $\alpha_{I\!P}(t)$ by (9).

We tune the Pomeron parameters $\alpha(0), \alpha'$ of (9) and a_1, a_2 of (12) so as to describe the high energy pp (or $p\bar{p}$) $\sigma_{\rm tot}$ and $d\sigma_{\rm el}/dt$ data. The dashed curve in Fig. 4 shows the description of $\sigma_{\rm tot}$. The dashed curves on Fig. 5 show the description of ISR and Tevatron elastic data, together with the prediction at the LHC energy. From Fig. 5 it is difficult to see the dependence of the *local* elastic slope, B of (2), with t, though the lack of constancy of B is clearly manifest in the ISR data. A much more visible way to explore the t dependence of B is to plot the ratio $(d\sigma_{\rm el}/dt)/\exp(B_{\rm expt}t)$ versus t, where $B_{\rm expt}$ is the experimentally measured elastic slope at small t. In other words we divide out the major part of the t dependence of the data. Figures 6–8 display the elastic data in this way at ISR, S$p\bar{p}$S and Tevatron energies, together with the model description (dashed curves). Although it is interesting to note that this physically motivated model explains the main features of the data, we delay the discussion of the detailed structure until we have extended the model of the Pomeron to allow for high-mass diffractive dissociation (which produces the continuous curves in Figs. 4–8). The parameters of the Pomeron corresponding to the dashed curves are[4]

$$\alpha(0) \;+\; \alpha' t = 1.102 \;+\; 0.066\; t\;,$$

[4] Note that if, instead of (12), we were to use a popular parametrization for $\beta(t)$, the best (but still not as detailed as

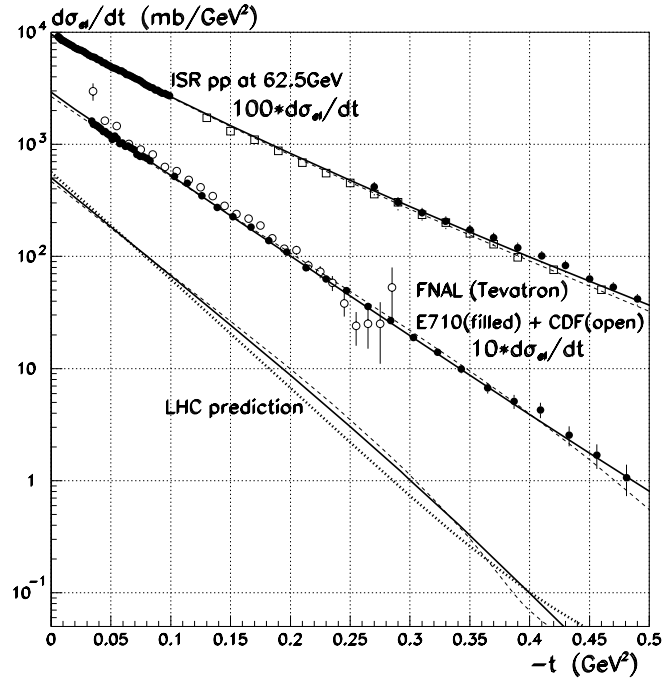

Fig. 5. The data for $d\sigma_{\rm el}/dt$ versus $|t|$ obtained at the ISR [13] and at the Tevatron [14,15], compared with the Pomeron model descriptions. The model predictions for $d\sigma_{\rm el}/dt$ at the LHC energy are also shown. The curves are as described in Fig. 4. (Note the inclusion of factors of 100 and 10 at the ISR and Tevatron energies respectively)

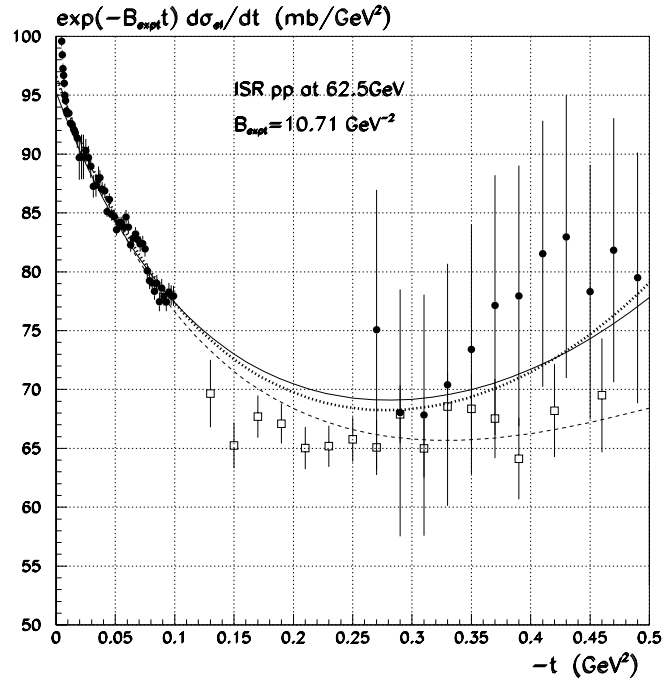

Fig. 6. ISR data [13] for $d\sigma_{\rm el}/dt$, with the experimental exponential form divided out, compared with the description of models of the Pomeron with high-mass diffraction included (continuous and dotted curves) and neglected (dashed curve). The influence of the Coulomb interaction, which we neglect, is evident in the data at very small t

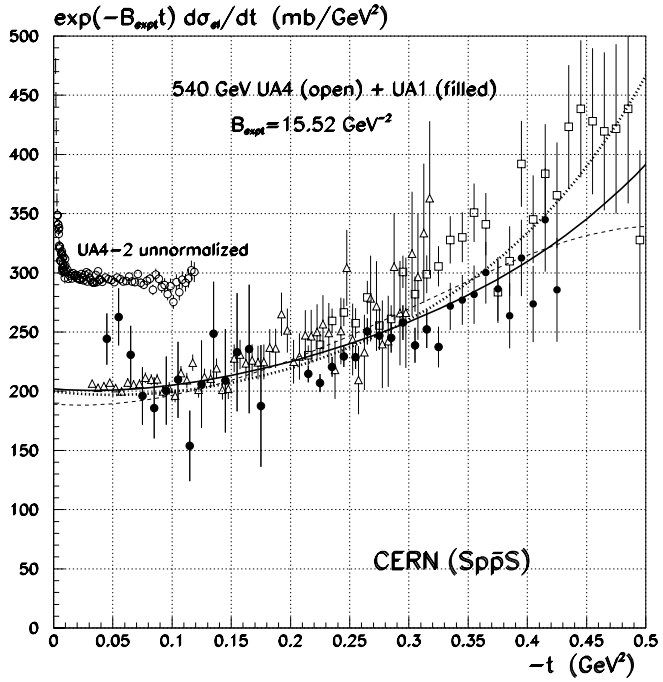

Fig. 7. As for Fig. 6, but showing S$p\bar{p}$S elastic data [16–18]. The most recent UA4 data [17] are unnormalized, and are plotted higher for clarity. These latter data show evidence of the Coulomb interaction at very small t, which lies outside our analysis

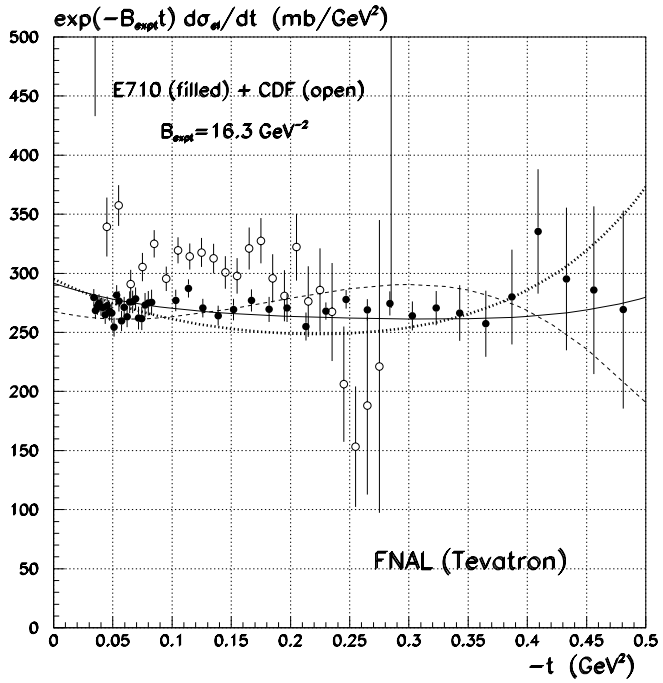

Fig. 8. As for Fig. 6, but showing Tevatron elastic data [14, 15]

$$a_1 \;=\; 0.48 \text{ GeV}^2, \quad a_2 \;=\; 3.6 \text{ GeV}^2, \tag{16}$$

with t in GeV^2. Remarkably, after the pion-loop insertions and eikonalization, (the 'small-distance' component of) the Pomeron looks similar to a fixed pole at $\alpha(0) = 1$; recall that when $h_\pi(0)$ of (11) is introduced, the bare pole trajectory $\alpha(0)$ is decreased by about 0.1. The shrinkage of the diffraction peak, which is conventionally described by an effective trajectory (7) with $\alpha' \simeq 0.25$ GeV^{-2}, actually is seen to have a dominant contribution from the pion-loop insertions in the trajectory and from the eikonal procedure. Moreover, the non-perturbative large distance pion-loop contribution explains almost all of the value of

$$\Delta \;\equiv\; \alpha_{\rm eff}(0) \;-\; 1 \;\simeq\; 0.08. \tag{17}$$

Interestingly, the small-distance component of the Pomeron[5], with $\alpha(0) \simeq 1$, is in agreement with the flat input gluon distribution obtained at $Q^2 \simeq 1-2$ GeV^2 in the global parton analyses, see, for example, Fig. 1 in [21].

At first sight the values of the vertex parameters of (16), with $a_1 \ll a_2$, look unusual. On the other hand, if we recall the two-gluon structure of the dominant short-distance component of the Pomeron, then the most likely configuration is to share the momentum transfer between two of the valence quarks of the proton. In such a case we expect a pole form for the proton form factor with a_1 of the order of the usual 0.71 GeV^2 of the electromagnetic dipole form factor. In fact, for such a quark-diquark configuration we would anticipate that a_1 was a little less than 0.71 GeV^2. However the price for such a configuration is that the second gluon propagator is of the form $1/(m^2 - t/4)$, where $m \sim 1$ GeV is the effective gluon mass. This gives $a_2 \sim 4$ GeV^2. Thus the form of the vertex, necessary to describe the data, has a natural physical interpretation.

5 The Pomeron, including diffractive dissociation

As we discussed in Sect. 2, diffractive dissociation is a non-negligible part of the total cross section at high energies. We therefore repeat the analysis of Sect. 4, but now incorporating the single- and double-diffractive dissociation processes of Figs. 1d and e. We use the triple-Pomeron formalism, in which the single- and double-diffractive cross sections are respectively

$$M^2\frac{d\sigma_{\rm SD}}{dtdM^2} = \frac{1}{16\pi^2}\beta^2(t)\beta(0)g_{3I\!P}(t) \times \left(\frac{M^2}{s}\right)^{1+\alpha_{I\!P}(0)-2\alpha_{I\!P}(t)} \left(\frac{s}{s_0}\right)^{\alpha_{I\!P}(0)-1} \tag{18}$$

$$\frac{d\sigma_{\rm DD}}{dy_1dy_2dt} = \frac{1}{16\pi^3}\beta^2(0)g^2_{3I\!P}(t) \times \exp\left((1+\alpha_{I\!P}(0)-2\alpha_{I\!P}(t))\Delta y\right) \times \left(\frac{s}{s_0}\right)^{\alpha_{I\!P}(0)-1} \tag{19}$$

where $M \equiv M_X$, $\beta(t)$ is the proton-Pomeron coupling of (12), and $g_{3I\!P}$ is the triple-Pomeron vertex. The rapidity difference $\Delta y \equiv |y_1 - y_2|$, where y_1 and y_2 denote the edges of the rapidity gap in the double dissociation process.

To be self-consistent we must use, in (18) and (19), the final Pomeron amplitude, with all the screening effects included. That is for each individual Pomeron line in the diffractive dissociation diagrams of Figs. 1d,e we must use the screened, rather than the bare, Pomeron. A good, and simple, approximation for the screened Pomeron trajectory is the effective trajectory of (7). In other words in the diffractive contributions of (18) and (19) we approximate $\alpha_{I\!P}(t)$ by $\alpha_{\rm eff}(t)$ of (7). That is, we use $\alpha' = 0.25$ GeV^{-2} in (45), (47), (18) and (19).

We compute $\sigma_{\rm SD}$ and $\sigma_{\rm DD}$ by integrating over t, and over the full available rapidity or M^2 intervals, assuming that the triple-Pomeron formalism is applicable for $\Delta y > 3$ and $M^2 > 9$ GeV^2. The lower mass region is already included in the two-channel eikonal calculation, which incorporates the N^* excitations.

Next we have to include the screening corrections to the diffractive processes shown in Figs. 1d,e. The procedure is described in Appendix B. Both the diffractive cross sections, $\sigma_{\rm SD}$ and $\sigma_{\rm DD}$, are given by (44), but with different slopes given by (45) and (47) respectively. The crucial parameter is the size of the triple-Pomeron coupling. We choose the coupling, $g_{3I\!P}(0)$, to be in agreement with high-mass single diffractive dissociation cross section measured by the CDF collaboration, $2\sigma_{\rm SD} = 7.4 \pm 0.5$ mb [22].

Due to the logarithmically large dM^2/M^2 or dy_1dy_2 intervals which become available with increasing energy, the diffractive cross sections $\sigma_{\rm SD}$ and $\sigma_{\rm DD}$ increase rapidly, and their contribution may exceed the inelastic contribution described by the Pomeron pole. In this domain the corrections coming from higher order Reggeon graphs become important. In [23] it was shown that the sum of a subset of multi-Pomeron diagrams (the so-called 'fan' diagrams) have the effect of renormalizing the diffractive dissociation contribution Ω_D in the following way

$$\Omega_D(b_t) \;\to\; \frac{\Omega_D(b_t)}{1 + c\Omega_D(b_t)/\Omega_{I\!P}(b_t)}, \tag{20}$$

where $\exp(-\Omega_{I\!P})$ is the eikonal in the absence of (high-mass) diffraction and $\Omega_D(b_t)$ is equal to the diffraction cross section, (18) or (19), written in the impact parameter, b_t, representation. That is, $\Omega_D(b_t)$ is the Fourier transform of either (18) or (19) integrated over M^2 and screened by the two-channel eikonal with $\Omega = \Omega_{I\!P}(b_t)$, as described in Appendix B.

We stress that the above subset of multi-Pomeron diagrams is an incomplete summation[6]. If we choose $c = 2$ in

(12)) description of the existing data is achieved by using the proton Dirac form factor, $F_1(t)$, as proposed in [19].

[5] This may possibly mean that for probes corresponding to the scale $Q^2 \simeq 1-2$ GeV^2 we have reached the black disk limit, implying gluon saturation. Another possibility is that this component is the two-gluon Pomeron discussed by Low and Nussinov [20].

[6] Another prescription was proposed in [24] in which a series of multi-Pomeron vertices $g_{n I\!P \to m I\!P}$ was considered, assuming

(20) then we obtain eventual saturation of the diffractive cross sections, with increasing $\sqrt{s}$, at the Pumplin bound $\sigma_{\rm D}/\sigma_{\rm tot} = 0.5$ [26]. This choice may be considered as a lower limit for high-mass diffractive effects. However the Pumplin bound is not justified in the presence of high-mass diffractive dissociation. So as the other extreme we may set $c = 0$ in (20) and restrict ourselves to the simplest single- and double-diffractive dissociation contributions of Figs. 1d and e. We will take these two choices of higher-order $g_{3I\!P}$ contributions to demonstrate the range of uncertainty arising from the introduction of diffractive dissociation into the analysis. Diffractive dissociation becomes increasingly likely with increasing collider energy $\sqrt{s}$, and so it is particularly important to investigate the allowed range of the predictions at the LHC energy.

The $c = 2$ choice, which provides saturation of $\Omega_{\rm D}$, leads to smaller cross sections. We will call it the *minimal* diffractive choice. The alternative $c = 0$ analysis, where we neglect all $g_{3I\!P}$ higher-order multi-Pomeron graphs, we call the *maximal* diffractive choice.

Finally, after $\Omega_{\rm D}$ has been screened by the two-channel eikonal with $\Omega_{I\!P}$, we have to add it to $\Omega_{I\!P}$ to obtain the full eikonal for the elastic amplitude. For the two alternative choices, $c = 0$ and $c = 2$ in (20), we use the resulting full eikonals to calculate the real and imaginary parts of the amplitude $A_{\rm el}$ and the diffractive cross sections $\sigma_{\rm SD}$ and $\sigma_{\rm DD}$, as described in the Appendices.

6 Description of soft diffraction by the Pomeron

We are now able to extend the description of the $\sigma_{\rm tot}$ and $d\sigma_{\rm el}/dt$ data, that we presented in Sect. 4, to include the effects of (high-mass) diffractive dissociation. In comparison to our 'first look' at the data, we now have two extra parameters: the triple-Pomeron coupling $g_{3I\!P}(0)$ and its slope b', see (46). We choose these parameters so as to be in reasonable agreement with the data on single-diffractive dissociation [22]. The data indicate that the slope is very small and so we explore values in the small b' domain. In the absence of screening, the data require [7, 8] $g_{3I\!P}(0)/\beta(0) \sim 0.025 - 0.05$, where, as usual, $\beta(0)$ is the proton-Pomeron coupling. However, after the rescattering effects are included, a much larger value of the triple-Pomeron vertex is needed in order to describe the same data, namely

$$g_{3I\!P}(0)/\beta(0) \simeq 0.25 \quad \text{or} \quad 0.15, \tag{21}$$

according to whether the minimal ($c = 2$) or maximal ($c = 0$) diffraction dissociation model is adopted.

We tune all six parameters $(\alpha(0), \alpha', a_1, a_2$ of (9) and (12), together with $g_{3I\!P}(0)$ and $b')$ to describe the $\sigma_{\rm tot}$ and $d\sigma_{\rm el}/dt$ data. The values of the first four do not differ appreciably from those obtained in the simplified model of Sect. 4, in which high-mass diffraction was neglected. For the minimal diffractive model we obtain

$$\alpha(0) \, + \, \alpha' t = 1.103 \, + \, 0.00 \, t \, , \tag{22}$$

$$a_1 \, = \, 0.47 \text{ GeV}^2, \quad a_2 \, = \, 2.6 \text{ GeV}^2, \tag{23}$$

as compared to the values in (16). Essentially the same values of these parameters are obtained in the maximal diffractive model (but with $a_2 = 2.4$ GeV^2). The two models really only differ in the values of the diffractive parameters. The triple-Pomeron coupling is given by (21) and the slope $b' = 0$ or 1 GeV^{-2} according to whether we use the minimal or maximal diffractive model.

Again the agreement with the $\sigma_{\rm tot}$ and $d\sigma_{\rm el}/dt$ data is good throughout the ISR to Tevatron energy range. The continuous and dotted curves in Figs. 4–8 show the description obtained if diffractive dissociation is included using the minimal and maximal models respectively. Recall that after dividing by $\exp(B_{\rm expt}t)$, where $B_{\rm expt}$ is the experimental slope at small t, Figs. 6–8 display very fine detail of the structure of the elastic differential cross section. It is remarkable that, with a minimal number of physically motivated parameters, the Pomeron is able to describe all the essential features of the data throughout the ISR to Tevatron energy interval.

The two models have, by definition, differing amounts of diffractive dissociation. The cross section for high-mass single-diffractive dissociation at $\sqrt{s} = 1.8$ TeV is

$$2\sigma_{\rm SD} \, = \, 5.3 \quad \text{or} \quad 8.0 \text{ mb} \tag{24}$$

in the minimal and maximal models respectively, as compared to the experimental value of 7.4±0.5 mb [22]. In fact it was not possible to reach the observed value of $\sigma_{\rm SD}$ using the minimal model with diffractive dissociation which saturates at the Pumplin bound. From this viewpoint we see that the two models should give a realistic, if generous, guide to the uncertainties associated with the effects of including diffractive dissociation.

The influence of diffractive dissociation is rather small at ISR energies, but it increases to given an appreciable effect at Tevatron and LHC energies. It can be seen from Fig. 9 that diffractive dissociation enlarges the spatial extent of the interaction and, as a consequence, increases the value of the elastic slope B. This is particularly true at LHC energies where there are, as yet, no data. At lower energies the potential change in the value of B is somewhat compensated in that we have to tune the parameters of the model to describe the *same* data. Differences occur in the predictions of the minimal and maximal models when we extrapolate beyond the available data — compare the continuous and dotted curves for $\sigma_{\rm tot}$ in Fig. 4 and, again, for ${\rm Re}A_{\rm el}/{\rm Im}A_{\rm el}$ in Fig. 10a.

The derivative dB/dt at $t = 0$ becomes smaller as $\sqrt{s}$ increases, reaching approximately zero at LHC energies, see Fig. 9. For the maximal choice of diffractive dissociation, where the change induced is larger, it even alters the sign of dB/dt at $t = 0$ at $\sqrt{s} = 14$ TeV. It is interesting to note that the pion-loop insertions into the bare Pomeron trajectory leads to a change of slope

$$\Delta B \, \equiv \, B(0) \, - \, B(t = -0.2 \text{ GeV}^2) \tag{25}$$

specific analytic forms for the n and m dependences; see also [25]. Qualitatively, this prescription produces more or less the same saturation of the diffractive cross section.

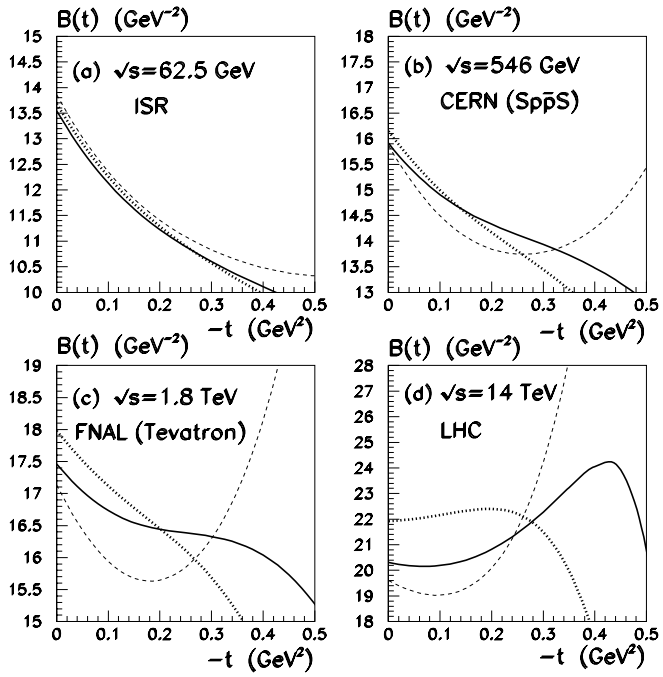

Fig. 9a–d. The model predictions for the t dependence of the local elastic slope, (2), at pp (or $p\bar{p}$) collider energies of **a** 62.5 GeV, **b** 546 GeV, **c** 1.8 TeV and **d** 14 TeV. The continuous, dotted and dashed curves correspond, respectively, to the minimal, maximal diffractive models and to the model of the Pomeron in which high-mass diffraction is neglected. The modification of $B(t)$ near the diffractive minimum, due to the inclusion of high-mass diffraction, increases with $\sqrt{s}$, reflecting the growth of this diffractive component

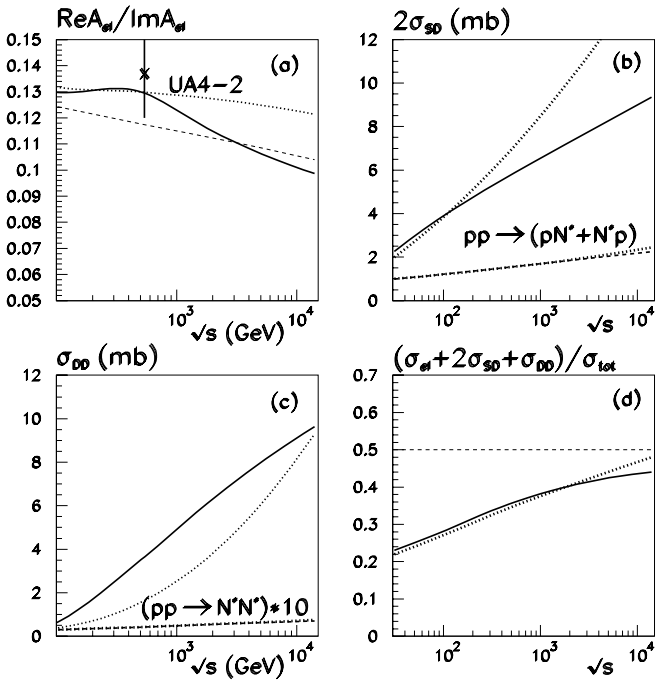

Fig. 10. a The predictions for the real to imaginary ratio of the pp (or $p\bar{p}$) elastic amplitude $A_{\rm el}$, compared to the UA4 measurement [17]. The curves are as described in Fig. 9. **b** The *total* single-diffractive cross section including the N^* excitation contribution (which is also plotted separately). **c** The double-diffractive cross section including the very small N^*N^* excitation contribution (which is plotted separately, multiplied by 10). **d** The prediction for the fraction of $\sigma_{\rm tot}$ that is diffractive compared to the Pumplin bound (dashed line)

which increases with $\sqrt{s}$, and which reaches a value $\Delta B = 1.3$ GeV^{-2} at the LHC energy. When, in addition, the Pomeron-proton form factor (12) is used (rather than an exponential form) then the difference ΔB increases to 3.8 GeV^{-2}. However these effects are masked by the inclusion of rescattering corrections so that, finally, by coincidence, $\Delta B \simeq -0.5$ GeV^{-2} for all models at the LHC energy, see Fig. 9d.

A 'good message' is that the inclusion of diffractive dissociation suppresses the growth of $B(t)$ as the diffractive dip is approached. The steep rise of the dashed curves, due to the cancellation between the Pomeron pole and cut contributions, is affected by the interplay with the diffractive amplitudes, which have their own interference producing a minimum at a different t value. Thanks to this effect, we predict only a small variation of the local elastic slope in the $|t| < 0.1$ GeV^2 domain at LHC energies, see Fig. 9d.

In Fig. 10a we show the energy dependence of the ratio of the real to the imaginary part of the elastic amplitude. We emphasize that we consider only even-signature Pomeron amplitudes, and that we have neglected odd-signature odderon exchange. Little is known about the strength of the odderon, however it could increase the real part of the $p\bar{p}$ amplitude measured by the UA4 collaboration [17] such that $\mathrm{Re}\, A_{\rm el}/\mathrm{Im}\, A_{\rm el}$ increases by up to 0.01. Correspondingly, the prediction for pp elastic scattering would decrease.

Figure 10b shows the energy dependence of the *total* single-diffractive dissociation cross section $2\sigma_{\rm SD}$, which also includes the N^* excitation contribution. The factor of 2 allows for diffraction of either the target or the beam proton. In a similar way, in Fig. 10c we show the double-diffractive dissociation cross section, together with its N^*N^* component. Finally, in Fig. 10d we present the ratio of the total diffractive cross section to $\sigma_{\rm tot}$, showing the approach to the Pumplin bound with increasing energy.

7 Survival probabilities of rapidity gaps

Our approach allows the calculation of the survival probabilities of the rapidity gaps which feature in the various diffractive processes. The rapidity gaps, which naturally occur whenever we have (colourless) Pomeron exchange, tend to get populated by secondary particles from the underlying event. Since, here, we have incorporated the effects of rescattering in some detail, we are able to calculate the survival probabilities S^2 of the gaps. There has recently been much interest in the size of S^2 [27,28], because of the possibility of extracting New Physics from

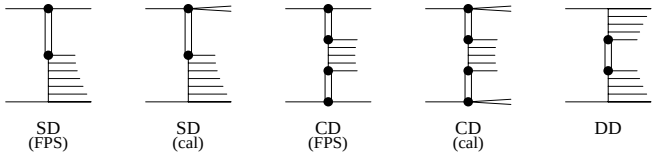

Fig. 11. The survival probability S^2 of the rapidity gaps (associated with the Pomeron, shown by the double vertical line) is calculated for these five diffractive processes. SD, CD, DD denote single, 'central' and double diffraction. FPS or cal denote 'forward proton spectrometer' or 'calorimeter', and correspond, respectively, to the detection of isolated protons, or to events where the leading baryon is either a proton or a N^* (shown symbolically as two lines emerging from the vertex)

hard diffractive processes in an almost background-free environment and, from a theoretical viewpoint, because of its reliance on subtle QCD techniques.

Again, it is convenient to work in impact parameter, b_t, space. Let $\mathcal{M}(s, b_t)$ be the amplitude of the particular diffractive process of interest. Then the probability that there is no extra inelastic interaction is

$$S^2 \;=\; \frac{\int |\mathcal{M}(s,b_t)|^2\, e^{-\Omega(b_t)}\, d^2b_t}{\int \mathcal{M}(s,b_t)|^2\, N d^2b_t}, \qquad (26)$$

where, as usual, Ω is the opacity (or optical density) of the interaction[7]. The normalizing factor $N = \exp(-\Omega^0)$, where Ω^0 denotes the relevant opacity ((48)–(52)) evaluated at $\Omega = 0$. The opacity $\Omega(b_t)$ reaches a maximum in the centre of the proton and becomes small in the periphery. Therefore the survival probability S^2 depends strongly on the spatial distribution of the constituents of the relevant subprocess. As examples we consider single and double rapidity gap processes, assuming that the spatial (b_t) distribution is controlled by the slope[8] b of the Pomeron-proton vertex ($\beta(t) \propto \exp(bt)$), and that there is no shrinkage coming from the Pomeron amplitude associated with the gap(s). This is the case for hard diffractive subprocesses[9].

[7] For simplicity we first discuss the simple one-channel eikonal approximation. The exact formulas for the two-channel eikonal are given in the Appendices.

[8] Here we again approximate (12) by an exponential form, see also (46).

[9] The amplitude which generates a large rapidity gap in a hard diffractive process is not the same as that for soft diffraction. It selects the small size component of the Pomeron, which has a negligible value of α'. For instance, the diffractive central production of a Higgs boson or high-E_T dijets or diffractive heavy vector meson production, are all hard diffractive processes that are driven by the *skewed* gluon distribution which is evolved from an input scale $Q_0 \sim m$ up to the hard scale, μ_H, characteristic of the diffractive process. Therefore it can be shown [29] that $\alpha' \sim \alpha_S/\mu^2$, where μ is the running evolution scale. During the evolution μ increases up to μ_H, and so, at leading order, we have $\alpha' \simeq 0$.

Table 1. The survival probabilities S^2 of rapidity gaps in single, central, double diffractive processes at S$p\bar{p}$S, Tevatron and LHC energies calculated using the minimal diffractive dissociation model of the Pomeron. The processes are shown in Fig. 11.

		Survival probability S^2 for:				
$\sqrt{s}$ (TeV)	$2b$ (GeV^{-2})	SD (FPS)	SD (cal)	CD (FPS)	CD (cal)	DD
0.54	4.0	0.14	0.13	0.07	0.06	0.20
	5.5	0.20	0.18	0.11	0.09	0.26
	7.58	0.27	0.25	0.16	0.14	0.34
1.8	4.0	0.10	0.09	0.05	0.04	0.15
	5.5	0.15	0.14	0.08	0.06	0.21
	8.47	0.24	0.23	0.14	0.12	0.32
14	4.0	0.06	0.05	0.02	0.02	0.10
	5.5	0.09	0.09	0.04	0.03	0.15
	10.07	0.21	0.20	0.11	0.09	0.29

We calculate the survival probability S^2 for three illustrative values of the slope $2b$ of the diffractive inclusive cross sections[10]:

(i) $2b = 4$ GeV^{-2}, in agreement with our parametrization of the Pomeron-proton vertex (compare (12) and (23) with (46)),
(ii) $2b = 5.5$ GeV^{-2}, which corresponds to the slope of the electromagnetic proton form factor,
(iii) $2b = B/2$, which is the elastic slope at the corresponding energy.

Moreover we calculate S^2 for five different diffractive processes. We consider single- and double-diffractive dissociation (SD, DD), and a process which may be called *central* diffraction (CD), that is a centrally produced state X with rapidity gaps on either side. For both SD and CD we consider two possibilities: first with N^* excitation permitted (relevant to a forward calorimeter experiment, denoted cal) and, second, without N^* excitation (relevant to a forward proton spectrometer measurement, denoted FPS). The five diffractive processes are sketched in Fig. 11. The b_t dependences of the single- and double-diffractive dissociation amplitudes can be found in Appendix B. We find

$$|\mathcal{M}|^2 \;\propto\; \exp(-b_t^2/nb) \qquad (27)$$

where $n = 6, 8$ and 4 for SD, DD and CD respectively. Thus double-diffraction has the largest spatial extent.

In practice we use the full two-channel expressions for the screening factors, which are collected together in (48)–(52) of Appendix B. Using these screening factors in (26), together with the appropriate amplitudes, we find the gap survival probabilities S^2 that are shown in Table 1.

There are several comments relevant to the survival probabilities listed in Table 1. *First*, we see that the results with and without the detection of the N^* excitations

[10] Note that the t dependence of the leading proton is given by $d\sigma/dM^2dt \propto \exp(2bt)$, see (18).

are very similar. *Second*, we see that the double-diffractive process, with a single rapidity gap in the central region, has the largest chance that the gap survives the rescattering, due to the wider spatial distribution of the basic process (see (27) with $n = 8$). *Third*, the gap survival probability S^2 decreases with $\sqrt{s}$ due to the growth of the opacity, but increases with the slope b as then a larger part of the basic subprocess extends to the periphery of the interaction. *Fourth*, we find that the survival probabilities listed in the Table are essentially unchanged if we use the maximal diffractive model, or even if we revert to the simple model of the Pomeron in which large mass diffraction is neglected. Recall that the parameters of all models are tuned to the *same* data, so major differences in the predictions are compensated.

The *fifth* comment concerns the calculation of S^2 for single-diffractive dissociation. Here we do not use the whole opacity $\Omega_{I\!P} + 2\Omega_{\rm SD} + \Omega_{\rm DD}$, but rather $\Omega_{I\!P} + \Omega_{\rm SD} + \Omega_{\rm DD}$. In this way we avoid single-diffractive dissociation which has a gap at the same location as that occurring in the diffractive process of interest. However it is worth noting that this subtle correction only gives a 5% enhancement in the predictions for S^2.

The *sixth* comment is that central diffractive processes, with two rapidity gaps, have the smallest survival probabilities. The predictions $S^2 = 0.08$ at the Tevatron and $S^2 = 0.04$ at the LHC, for $b = 5.5$ GeV^{-2}, are in agreement with our previous estimates [28] based on a more simplified model. The earlier work did not use a two-channel eikonal formalism to account for N^* excitations (but instead used a simplified excitation factor). Nor did it include pion-loop insertions or allow for high-mass diffractive processes. Nevertheless the stability of the predictions for S^2 is encouraging, and we expect the values given in Table 1 to be reliable estimates of the effects of rescattering.

8 Conclusions

We have constructed a formalism that incorporates all the main features of high energy soft diffraction. First, we account for the nearest singularity produced by t-channel unitarity by including the *pion-loop* contributions in the bare Pomeron pole. In this way we correctly reproduce the behaviour of the diffractive amplitudes at large b_t, in the peripheral region of the interaction. Second, we use a *two-channel eikonal* to include the Pomeron cuts generated by elastic and quasi-elastic (with N^* intermediate states) s-channel unitarity. Finally, we incorporate high-mass *diffractive dissociation* in the whole procedure. To the best of our knowledge, no model has attempted to include all these effects simultaneously.

The model may be used to predict all soft diffractive processes at LHC energies. The main uncertainty is the size of diffractive dissociation. We consider two physically motivated extremes, which we called the minimal and maximal diffractive models, giving lower and upper bounds for the cross sections. At $\sqrt{s} = 14$ TeV we predict a total pp cross section in the range

$$\sigma_{\rm tot} \;=\; 99.1 - 104.5 \text{ mb}, \tag{28}$$

and a pp elastic differential cross section at $t = 0$

$$\frac{d\sigma_{\rm el}}{dt} \;=\; 506 - 564 \text{ mb/GeV}^2, \tag{29}$$

with a slope, at $t = 0$, of

$$B(0) \;=\; 20.3 - 21.9 \text{ GeV}^{-2}. \tag{30}$$

Also we find that the ratio of the real to the imaginary part of the elastic amplitude should lie in the range

$$\mathrm{Re}A_{\rm el}/\mathrm{Im}A_{\rm el} \;=\; 0.10 - 0.12, \tag{31}$$

at $\sqrt{s} = 14$ TeV. For the single- and double-diffractive dissociation cross sections we predict

$$\begin{aligned} 2\sigma_{\rm SD} &= 9.4 - 15.4 \text{ mb}\,, \\ \sigma_{\rm DD} &\simeq 9.5 \text{ mb}, \end{aligned} \tag{32}$$

which include N^* excitation contributions of 2.3 and 0.1 mb respectively.

We are also able to make reliable predictions for the probability S^2 that the large rapidity gaps (which characterise diffraction) survive the soft rescattering corrections, that is survive the population of the gap by secondary particles from the underlying event. These probabilities decrease with collider energy due to the growth of the opacity Ω of the interaction. Moreover they depend on the particular diffractive interaction of interest and on the configuration of the rapidity gaps (as demonstrated by Table 1 and Fig. 11). For example, for double-diffractive central Higgs production via WW fusion we predict $S^2 = 0.08(0.04)$ at Tevatron (LHC) energies. Since the W boson, like the photon, is radiated from a quark, it is natural to choose the slope $2b$ in Table 1 to be that of the electromagnetic form factor, $2b = 5.5$ GeV^{-2}. On the other hand for the production of a Higgs by Pomeron-Pomeron fusion it is natural to choose $2b = 4$ GeV^{-2}, consistent with our Pomeron-proton vertex. In this case the depletion $S^2 = 0.05(0.02)$ at Tevatron (LHC) energies.

It is interesting to note that, after all the effects (pion-loop, rescattering, diffractive dissociation) are simultaneously included, the pp $\sigma_{\rm tot}$ and $d\sigma_{\rm el}/dt$ data require both $\Delta \equiv \alpha(0) - 1$ and α' to be essentially zero for the *bare* Pomeron pole. Diffractive dissociation is more important in the periphery of the interaction and has the effect of "eating up" α' as can be seen by comparing $\alpha' = 0.07$ GeV^{-2} of (16), obtained with the simplified model, with the value $\alpha' \simeq 0$ of (22) when diffraction dissociation is included. Recall that soft processes are driven by two scales — the pseudo-Goldstone m_π scale and the normal hadronic scale $m \sim 1$ GeV. The interactions driven by the larger scale m should link up with perturbative QCD. Indeed we obtain $\alpha(0) \simeq 1$ for the small-size component of the Pomeron, in agreement with the flat gluon distribution obtained in global analyses for $Q^2 \simeq 2$ GeV^2. The

non-perturbative large-size component, arising from the pion-loop insertions, then shifts the Pomeron trajectory from $\alpha(0) \simeq 1$ to $\alpha_{I\!P}(0) \simeq 1.1$.

As mentioned above, the main uncertainty is in the treatment of diffractive dissociation. The two extreme treatments give results shown by the continuous and dotted curves in Figs. 4–10. The values of $\sigma_{\rm tot}$ and $d\sigma_{el}/dt$ are in agreement with results of simpler models [30], which account only for elastic s-channel unitarity. The major reason for the agreement is that the parameters of the models are tuned to describe the same data. It was shown in [24] that the introduction of diffractive dissociation can, to a large extent, be compensated by the renormalization of the parameters of the bare Pomeron. (Indeed it is interesting to note that the original predictions of [24] for $\sigma_{\rm tot}$, B and $\sigma_{\rm SD}$ are in excellent agreement with those of our maximal diffraction model.) However the contribution of diffractive dissociation is not negligible and reveals itself in the 'shoulder' seen in ${\rm Re}A_{\rm el}/{\rm Im}A_{\rm el}$ of Fig. 10a and in the extra curvature in Fig. 10d, using the minimal model which satisfies the Pumplin bound. From this point of view, it is possible that at the LHC we will enter a new domain in the high energy behaviour of soft diffraction. Either high-mass diffractive dissociation will saturate at the Pumplin bound, or it will continue to increase with the interaction dominantly occurring in the peripheral region, originating from processes with many rapidity gaps. Recall that the Pumplin bound is not justified in the presence of high-mass diffractive dissociation.

Of course, for any model with Pomeron cuts or driven by more than one Regge pole, we should not expect factorization. However, as has been known for a long time [23], if, by chance, approximate factorization should occur at some high energy, then it will be valid over a rather large energy interval on account of the 'flat' energy behaviour of the amplitudes.

Here we have considered only the positive signature contributions and have neglected odderon exchange. The normalisation of the odderon contribution is unknown. However it is described by three, or more, gluon exchange, and so a flatter t dependence is expected for this amplitude. It could well reveal itself for $|t| \gtrsim 0.5$ GeV^2.

In conclusion, we have constructed a formalism for soft interactions, driven by the Pomeron, that embodies all the major physical effects. We therefore believe that it should give reliable predictions for all soft diffractive phenomena at the LHC, at least in the $|t| \lesssim 0.5$ GeV^2 domain.

Acknowledgements. We thank Mike Whalley for collecting and preparing the data, and A.B. Kaidalov, E.M. Levin, V. Nomokonov, R. Orava and S. Tapprogge for useful discussions. VAK thanks the Leverhulme Trust for a Fellowship. This work was also supported by the Royal Society, PPARC, the Russian Fund for Fundamental Research (98-02-17629) and the EU Framework TMR programme, contract FMRX-CT98-0194 (DG 12-MIHT).

Appendix A: the two-channel eikonal

In this work we have used a two-channel eikonal [11] in which, besides the elastic proton channel, we allow proton excitation N^* to be a possible intermediate state in pp elastic scattering, as in Fig. 1c. This *effective* N^* channel describes the sum of low mass diffractive proton excitations. For the various p and N^* couplings to the Pomeron we take a common[11] t dependence of the form of (12), but with

$$\beta_p \to \begin{pmatrix} \beta(p\to p) & \beta(p\to N^*) \\ \beta(N^*\to p) & \beta(N^*\to N^*) \end{pmatrix} \simeq \beta(p\to p) \begin{pmatrix} 1 & \gamma \\ \gamma & 1 \end{pmatrix} \tag{33}$$

where γ is given by (13). That is we assume that pp and N^*N^* interactions have the same cross sections, as suggested by the additive quark model. Indeed Gribov [31] has argued that all hadrons have the same elastic interaction with the bare Pomeron and, moreover, he predicted that γ is small due to the orthogonality of the quark wave functions of the p and N^*. Of course, the Pomeron interaction produces some distortion of the original form of the baryon wave functions, giving $\gamma \neq 0$.

We see that the eigenvalues of the above two-channel vertex are $1\pm\gamma$. Now each amplitude has two vertices and so, for example, the total and elastic pp cross sections,

$$\sigma_{\rm tot} = 2\int d^2b_t\, A_{\rm el}(b_t)$$
$$\sigma_{\rm el} = \int d^2b_t\, |A_{\rm el}(b_t)|^2, \tag{34}$$

are controlled by an elastic amplitude, $A_{\rm el}$, with three different exponents

$${\rm Im}A_{\rm el}(b_t) = \Big[1 - \frac{1}{4}e^{-(1+\gamma)^2\Omega/2} - \frac{1}{2}e^{-(1-\gamma^2)\Omega/2} - \frac{1}{4}e^{-(1-\gamma)^2\Omega/2}\Big]. \tag{35}$$

As usual, $\Omega \equiv \Omega(s,b_t)$ is the optical density (or opacity) of the interaction. Similarly, the single- and double-excitation amplitudes are given by

$${\rm Im}\,A(pp\to N^*p) = \frac{1}{4}\Big[e^{-(1-\gamma)^2\,\Omega/2} - e^{-(1+\gamma)^2\,\Omega/2}\Big]$$
$${\rm Im}\,A(pp\to N^*N^*) = \frac{1}{4}\Big[e^{-(1-\gamma)^2\,\Omega/2} - 2\,e^{-(1-\gamma^2)\,\Omega/2} + e^{-(1+\gamma)^2\,\Omega/2}\Big]. \tag{36}$$

The opacity is chosen to be real, and the real parts of the amplitudes are calculated from

$$\frac{{\rm Re}\,A}{{\rm Im}\,A} = \tan\left(\frac{\pi\lambda}{2}\right) \tag{37}$$

[11] So as to keep the number of parameters minimal.

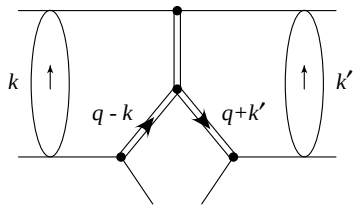

Fig. 12. Screening corrections to the triple-Pomeron diagram of Fig. 1d

where

$$\lambda \;=\; \frac{\partial \ln(\mathrm{Im}\, A)}{\partial \ln s}. \tag{38}$$

This is a simple way of implementing the dispersion relation determination of the real part of the amplitude.

For the case of one-channel (pure elastic) rescattering we have $\gamma = 0$, and hence

$$\mathrm{Im}\, A_{\rm el} \;=\; [1 - e^{-\Omega/2}]. \tag{39}$$

Just for illustration, assume that we have an effective Pomeron with a linear trajectory

$$\alpha_{\rm eff}(t) \;=\; 1 \,+\, \Delta \,+\, \alpha' t, \tag{40}$$

and a vertex with exponential t dependence of the form $\beta_p \exp(B_0 t/4)$, corresponding to an elastic slope B_0. Then the opacity

$$\Omega(s, b_t) \;=\; \frac{\beta_p^2 (s/s_0)^{\Delta}}{4\pi B_P}\, e^{-b_t^2/4B_P}, \tag{41}$$

where the slope of the Pomeron amplitude is

$$B_P \;=\; \frac{1}{2} B_0 \,+\, \alpha' \,\ln(s/s_0). \tag{42}$$

In the calculations presented in this paper we do not use the above simple exponential form leading to the opacity of (41), but rather the opacity obtained from the numerical Fourier transform of the Pomeron exchange amplitude of (15).

Appendix B: screening effects in diffractive dissociation

Here we describe how to calculate the screening corrections to the single- and double- diffractive processes shown in Figs. 1d,e. For single diffraction, for example, we need to compute the eikonal rescattering effects indicated by the blobs with momentum transfer k and k' in Fig. 12. It is most convenient to work in impact parameter b_t space.

For simplicity we assume an exponential form for the 't' dependences of the vertices. For example, for the single-diffractive process of Fig. 12 we assume that the unscreened amplitude squared has the form

$$\exp\left[-C(k+q)^2 - C(k'-q)^2 - C'(k+k')^2\right]. \tag{43}$$

Using this form, the cross section is evaluated to be

$$\sigma_{\rm SD} \;=\; \frac{\sigma_{\rm SD}(0)}{4C(2C'+C)} \int e^{-\Omega} \exp\left(-\frac{b_t^2}{4C'+2C}\right) db_t^2 \tag{44}$$

where we have included the (single-channel) eikonal screening effect $\exp(-\Omega)$. $\sigma_{\rm SD}(0)$ is the single-diffractive differential cross section evaluated at $t = 0$ (in the absence of screening). The slopes are

$$\begin{aligned} C' &= b + b' + \alpha' \,\ln(M^2/s_0) \\ C &= b + b' + \alpha' \,\ln\left(s/M^2\right), \end{aligned} \tag{45}$$

where b and b' are the slopes of the proton-Pomeron and triple-Pomeron vertices respectively, that is

$$\beta(t) \;\propto\; e^{bt}, \qquad g_{3I\!P}(t) \;\propto\; e^{b't}. \tag{46}$$

The double diffractive cross section $\sigma_{\rm DD}$ has an identical form to (44), except that now we have $\sigma_{\rm DD}(0)$ and different slopes

$$\begin{aligned} C' &= 2b + 2b' + \alpha' \left(\ln\frac{s}{s_0} - \Delta y\right), \\ C &= 2b' \,+\, \alpha' \,\Delta y. \end{aligned} \tag{47}$$

We take the slope of the proton-Pomeron vertex to be $b = 2\ \mathrm{GeV}^{-2}$, which well approximates the form given by (12) and (23). The data indicate that the slope of the triple-Pomeron vertex is very small.

The screening factor $\exp(-\Omega)$ in the two-channel (p, N^*) eikonal model becomes, for single-diffraction,

$$\begin{aligned} e^{-\Omega} \to \frac{1}{4} \Big\{ &(1+\gamma)^3 e^{-(1+\gamma)^2\Omega} \,+\, (1-\gamma)^3 e^{-(1-\gamma)^2\Omega} \\ &+ 2(1-\gamma^2) e^{-(1-\gamma^2)\Omega} \Big\}, \end{aligned} \tag{48}$$

and for double-diffraction

$$\begin{aligned} e^{-\Omega} \to \frac{1}{4} \Big\{ &(1+\gamma)^2 e^{-(1+\gamma)^2\Omega} \,+\, (1-\gamma)^2 e^{-(1-\gamma)^2\Omega} \\ &+ 2(1-\gamma^2) e^{-(1-\gamma^2)\Omega} \Big\}, \end{aligned} \tag{49}$$

where γ is given by (13). These structures incorporate the interference of the eigenvectors $p \pm N^*$ with absorptive cross sections proportional to $1 \pm \gamma$. In the case of single diffraction, (48) includes the possibility of the $p \to N^*$ transition for the fast (i.e. lower) proton in Fig. 12.

In Sect. 7 we calculate the chance that the rapidity gaps occuring in five different diffractive processes survive after the rescattering effects are included. The five processes are shown in Fig. 11. We therefore need five different screening factors. The factors (48) and (49) correspond to two of the processes, namely SD(cal) and DD respectively. For single-diffractive dissociation in which an isolated proton is detected using a forward proton spectrometer, SD(FPS), we have

$$e^{-\Omega} \to \frac{1}{8} \Big\{ (1+\gamma) \Big[(1+\gamma)\, e^{-(1+\gamma)^2\ \Omega/2}$$

$$+ (1-\gamma)\, e^{-(1-\gamma^2)\,\Omega/2}\Big]^2 + (1-\gamma) \times \Big[(1-\gamma)\, e^{-(1-\gamma)^2\,\Omega/2} + (1+\gamma)\, e^{-(1-\gamma^2)\,\Omega/2}\Big]^2\Big\}. \quad (50)$$

For central diffraction with the detection of isolated protons, which we denoted CD(FPS), we have

$$e^{-\Omega} \to \frac{1}{16}\Big\{(1+\gamma)^2\, e^{-(1+\gamma)^2\,\Omega/2} + (1-\gamma)^2 \times e^{-(1-\gamma)^2\,\Omega/2} + 2(1-\gamma^2)\, e^{-(1-\gamma^2)\,\Omega/2}\Big\}^2, \quad (51)$$

whereas if either a p or a N^* may be detected using, say, a forward calorimeter, then we obtain for CD(cal)

$$e^{-\Omega} \to \frac{1}{4}\Big\{(1+\gamma)^4\, e^{-(1+\gamma)^2\,\Omega} + (1-\gamma)^4\, e^{-(1-\gamma)^2\,\Omega} + 2(1-\gamma^2)^2\, e^{-(1-\gamma^2)\,\Omega}\Big\}. \quad (52)$$

Note that when $\gamma \to 0$, all the formulae (48)–(52) reduce to the single-channel screening factor $\exp(-\Omega)$, as indeed they must.

References

1. See, M.M. Block, K. Kang and A.R. White, Int. J. Mod. Phys. **A7** (1992) 4449, for a collection and discussion of elastic data
2. A.A. Anselm and V.N. Gribov, Phys. Lett. **B40** (1972) 487
3. P.D.B. Collins, Regge Theory and High Energy Physics, Cambridge Univ. Press (1977)
4. V.A. Abramovskii, V.N. Gribov and O.V. Kancheli, Sov. J. Nucl. Phys. **18** (1974) 308
5. A. Donnachie and P.V. Landshoff, Phys. Lett. **B296** (1992) 227
6. K. Goulianos, Phys. Rev. **D14** (1976) 1445
7. A.B. Kaidalov, V.A. Khoze, Yu.F. Pirogov and N.L. Ter-Isaakyan, Phys. Lett. **B45** (1973) 493; A.B. Kaidalov and K.A. Ter-Martirosyan, Nucl. Phys. **B75** (1974) 471
8. R.D. Field and G.C. Fox, Nucl. Phys. **B80** (1974) 367
9. B.Z. Kopeliovich, I.K. Potashnikova, B. Povh and E. Predazzi, Phys. Rev. Lett. **85** (2000) 507
10. A.B. Kaidalov, Sov. J. Nucl. Phys. **13** (1971) 401
11. A.B. Kaidalov, Phys. Rep. **50** (1979) 157; K.A. Ter-Martirosyan, ITEP preprints No. 70, 71 (1975); 7, 11, 133–135, 158 (1976)
12. G. Carboni et al., Nucl. Phys. **B254** (1985) 697; N.A. Amos et al., Nucl. Phys. **B262** (1985) 689; UA4 Collaboration: M. Bozzo et al., Phys. Lett. **B147** (1984) 392; UA5 Collaboration: G.J. Alner et al., Z. Phys. **C32** (1986) 153; E710 Collaboration: N.A. Amos et al., Nuovo Cim. **A106** (1993) 123; E811 Collaboration: C. Avila et al., Phys. Lett. **B445** (1999) 419; CDF Collaboration: F. Abe et al., Phys. Rev. **D50** (1994) 5550; UA4/2 Collaboration: C. Augier et al., Phys. Lett. **B344** (1995) 451
13. N. Kwak et al., Phys. Lett. **B58** (1975) 233; U. Amaldi et al., Phys. Lett. **B66** (1977) 390; L. Baksay et al., Nucl. Phys. **B141** (1978) 1
14. E710 Collaboration: N.A. Amos et al., Phys. Lett. **B247** (1990) 127
15. CDF Collaboration: F. Abe et al., Phys. Rev. **D50** (1994) 5518
16. UA4 Collaboration: R. Battiston et al., Phys. Lett. **B147** (1984) 385
17. UA4/2 Collaboration: C. Augier et al., Phys. Lett. **B316** (1993) 448
18. UA1 Collaboration: G. Arnison et al., Phys. Lett. **B128** (1982) 336
19. A. Donnachie and P. V. Landshoff, Nucl. Phys. **B231** (1984) 189; **B267** (1986) 690
20. F. E. Low, Phys. Rev. **D12** (1975) 163; S. Nussinov, Phys. Rev. Lett. **34** (1975) 1286; Phys. Rev. **D14** (1976) 296
21. A.D. Martin, R.G. Roberts, W.J. Stirling and R.S. Thorne, Eur. Phys. J. **C4** (1998) 463
22. CDF Collaboration: F. Abe et al., Phys. Rev. **D50** (1994) 5535
23. Ya.I. Azimov, V.A. Khoze, E.M. Levin and M.G. Ryskin, Nucl. Phys. **B89** (1975) 508
24. A.B. Kaidalov, L.A. Ponomarev and K.A. Ter-Martirosyan, Sov. J. Nucl. Phys. **44** (1986) 468
25. J.L. Cardy, Nucl. Phys. **B75** (1974) 413
26. J. Pumplin, Phys. Rev. **D8** (1973) 2899
27. E. Gotsman, E.M. Levin and U. Maor, Phys. Rev. **D60** (1999) 094011
28. V.A. Khoze, A.D. Martin and M.G. Ryskin, Eur. Phys. J. **C14** (2000) 525
29. E.M. Levin and M.G. Ryskin, Z. Phys. **C48** (1990) 231
30. M.M. Block, F. Halzen and B. Margolis, Phys. Rev. **D45** (1992) 839; M.M. Block, Nucl. Phys. **B** (Proc. Suppl.) **71** (1999) 378; M.M. Block, F. Halzen and T. Stanev, Phys. Rev. Lett. **83** (1999) 4926
31. V.N. Gribov, Sov. J. Nucl. Phys. **17** (1973) 313